Cobalt(II) and Zinc(II) Complexes of Hexamethylenetetramine as Single Source Precursors for their Metal Oxide Nanoparticles

Che Dieudonne Tabong[1], Agwara Moise Ondoh[1], Divine Mbom Yufanyi[2] & Josepha Foba[3]

[1] Department of Inorganic Chemistry, Faculty of Science, University of Yaounde I, Yaounde, Cameroon

[2] Department of Chemistry, Faculty of Science, The University of Bamenda, Bamenda, Cameroon

[3] Department of Chemistry, Faculty of Science, University of Buea, Cameroon

Correspondence: Agwara Moise Ondoh, Department of Inorganic Chemistry, Faculty of Science, University of Yaounde I, Yaounde, Cameroon. E-mail: agwara29@yahoo.com

Abstract

Co_3O_4 and ZnO nanoparticles with different morphologies were synthesised by the thermal decomposition of single source precursors obtained from readily available and eco-friendly starting materials (hexamethylenetetramine and metal nitrates). The precursors, which were characterized by elemental analysis, Fourier transform infrared spectroscopy (FTIR), X-ray diffraction and thermal gravimetric analysis, were calcined at 500ºC for 2 h, and the oxide samples obtained were characterized by FTIR, X-ray diffraction (XRD), field emission scanning electron microscopy (FESEM), transmission electron microscopy (TEM), selected area electron diffraction (SAED), and nitrogen physisorption. XRD showed that the oxides obtained were crystalline and free of extraneous impurity phases. The morphology of the nanoparticles obtained changed from cube-like (Co_3O_4) to hexagonal-prism like morphology (ZnO), while the particle size increased from 19.6 to 64.5 nm, respectively. The method used simple and cheap precursors, which should make it suitable for large-scale synthesis.

Keywords: Cobalt oxide, Zinc oxide, Nanoparticle, Thermal decomposition, Hexamethylenetetramine, XRD

1. Introduction

Metal oxide nanoparticles constitute a class of functional materials on which much attention has been focused recently due to their morphology and size-dependent physical and chemical properties (Devan, Patil, Lin, & Ma, 2012; Niederberger, 2007).

The size reduction of these metal oxides, which leads to novel properties that are different from those of the individual atoms as well as their bulk counterparts, makes them potential materials for application in the fields of catalysis, electronics, storage devices, gas sensors and magnetic resonance imaging (de Rivas, López-Fonseca, Jiménez-González, & Gutiérrez-Ortiz, 2012; Devan et al., 2012; Gomez & Tigli, 2013; Kahn et al., 2009).

Among these metal oxide nanoparticles, nanoscale cobalt and zinc oxides have received much scientific attention because they have interesting size-dependent physico-chemical properties for material as well as industrial applications. Cobalt oxide, especially the cubic Co_3O_4 phase with a spinel structure (Fd3m), is a p-type semiconductor which has been employed in several technological applications in the field of heterogeneous catalysis (Che, Liu, Fu, & Jiang, 2013; de Rivas et al., 2012), supercapacitors (Vijayakumar, Ponnalagi, Nagamuthu, & Muralidharan, 2013; H. Xu et al., 2014), anode materials in lithium ion rechargeable batteries (Huang et al., 2014; Rui et al., 2013), and magnetic materials (Moro, Yu Tang, Tuna, & Lester, 2013; Sharma & Jeevanandam, 2013).

ZnO is a thermally and chemically stable semiconducting material with a wide band gap of 3.37 eV and a large exciton binding energy of 60 meV at room temperature. It has found application in the domains of gas sensors, catalysis and optical devices (Faisal, Khan, Rahman, Jamal, & Abdullah, 2012; Gomez & Tigli, 2013; Guo & Peng, 2015; Hirai & Asada, 2005; Karami, Eskandari, Khodabakhshi, Hoseini, & Hashemian, 2013; Pál et al., 2012; Xiong, Ma, Wang, & Xia, 2011). ZnO is also biocompatible, nontoxic, chemically stable, and electrochemically active; properties which have enabled its application in biosensing (Gomez & Tigli, 2013).

Various methods have been employed for the morphology-controlled synthesis of Co_3O_4 and ZnO nanoparticles, which include microwave-assisted synthesis (Faisal et al., 2012; Vijayakumar et al., 2013), Chemical precipitation (Greene, Yuhas, Law, Zitoun, & Yang, 2006; Romo et al., 2011; Rui et al., 2013), hydrothermal (Dakhlaoui, Jendoubi, Smiri, Kanaev, & Jouini, 2009; Lester et al., 2012; Moro et al., 2013; Pál et al., 2012; Rui et al., 2013), sonochemical (Banerjee, Chakrabarti, Maitra, & Dutta, 2012), solvothermal synthesis (Y. Xu, Wang, Sun, Zhang, & Gao, 2010), pulsed layer deposition (Warang et al., 2012), and biosynthesis (Fu & Fu, 2015). These varied methods have led to nanoparticles with diverse morphologies like nanocubes (Lester et al., 2012), nanorods (Fu & Fu, 2015; Romo et al., 2011), nanospheres (Dakhlaoui et al., 2009; Darezereshki, Alizadeh, Bakhtiari, Schaffie, & Ranjbar, 2011; Hirai & Asada, 2005), nanowires (Greene et al., 2006), nanoflowers (Pál et al., 2012), and nanotubes (Li, Dou, & Bao, 2012).

These conventional methods, though successful, require specially designed and expensive equipment, extra purification steps, rigorous reaction conditions and/or relatively high temperatures. Some of the solution-based synthetic approaches employ surfactants and solvents which are toxic and not easily degraded in the environment. The synthesis of these nanomaterials with controlled size and shape is still a major challenge and large scale synthesis of phase pure Co_3O_4 and ZnO nanoparticles at relatively low temperatures, using readily available, environmentally benign and cost-effective precursors is a synthetic challenge. Thus, the preparation of cobalt oxide and zinc oxide nanoparticles by thermal decomposition of cobalt and zinc complexes becomes increasingly important mainly due to its cost-effectiveness, careful choice of precursors and calcination conditions, high yields, easy control of synthesis conditions, particle size, crystal structure, and purity. For example, the synthesis of metal oxide nanoparticles by the thermal decomposition of organometallic compounds or metal complexes has been reported (Ahmad, Ganguly, Ahmed, Ganguli, & Alhartomy, 2011; Huang et al., 2014; Kahn et al., 2009; Palacios-Hernández et al., 2012; Sharma & Jeevanandam, 2013). Porous Co_3O_4 with different morphologies has been prepared by the thermal decomposition of cobalt carbonates (300 - 500°C for 2 – 3 h) and oxalate precursors (400 - 500°C for 6 h) (Che et al., 2013; de Rivas et al., 2012; Nassar & Ahmed, 2011). Rivas *et al*. obtained Co_3O_4 by the direct calcination of cobalt nitrate and cobalt oxalate nanorods at 500°C (de Rivas et al., 2012). Co_3O_4 nanoparticles were obtained by solid-state thermal decomposition of a Schiff base complex $[CoL_3]$ (L = N-salicylidin-2-chloroethylimine) at 450°C under air atmosphere for 3 h (Khalaji, Nikookar, Fejfarova, & Dusek, 2014). Hongwei and co-workers prepared Co_3O_4 microdiscs by a thermal decomposition of cobalt oxalate at 400°C, obtained by the solvothermal reaction of cobalt nitrate and ammonium oxalate in anhydrous alcohol (Che et al., 2013). Co_3O_4 nanoparticles were prepared via the decomposition of the pentammine(carbonato)cobalt(III) nitrate precursor complex $[Co(NH_3)_5CO_3]NO_3 \cdot 0.5H_2O$ at low temperature (175°C) (Farhadi & Safabakhsh, 2012). Palacios-Hernandez *et al*. reported the synthesis of Cu and Co metal oxide nanoparticles by the thermal decomposition of the corresponding tartrate complexes $([M(C_4H_2O_6)_n]_m$, M = Cu(II), Co(II)) at 500°C for 5 h (Palacios-Hernández et al., 2012). Aghababazadeh *et al*. prepared ZnO nanoparticles by the thermal decomposition (170-380°C) of $ZnCO_3$ obtained by mechanochemical processing (Aghababazadeh, Mazinani, Mirhabibi, & Tamizifar, 2006). Hirai and co-workers obtained ZnO nanoparticles by the calcination of $Zn(OH)_2$ nanoparticles, which were prepared in a polyethylene glycol mono-4-nonylphenyl ether (NP-5)/cyclohexane reverse micellar system and incorporated into polyurea via an *in situ* polymerization of hexamethylene diisocyanate (Hirai & Asada, 2005). Rajesh *et al*. prepared ZnO nanoparticles by the mechanochemical synthesis of $ZnC_2O_4 \cdot 2H_2O$ nanoparticles followed by its thermal decomposition at 400°C (Rajesh, Vara Lakshmi, & Sunandana, 2012). Spherical ZnO nanoparticles have also been prepared by the thermal decomposition of $Zn_4(SO_4)(OH)_6 \cdot 0.5\ H_2O$ in air for 1 h at 825°C (Darezereshki et al., 2011).

The high costs, use of non-ecofriendly surfactants and solvents as well as the evolution of very toxic gaseous products during calcination, limits the use of some of these precursors. In continuation of our interest in the synthesis of phase pure metal oxide nanoparticles, we report herein a simple, environmentally benign and cost-effective method to synthesize Co_3O_4 and ZnO nanoparticles by the thermal decomposition of their respective metal-hexamethylenetetramine (M-HMTA) complexes. Hexamethylenetetramine (HMTA) is a cheap, ecofriendly and readily available heterocyclic organic compound with a cage-like structure. It is highly soluble in water and polar organic solvents. Some metal complexes of HMTA had previously been used as precursors for metal dispersions (Afanasiev et al., 2008), metal carbides and nitrides (Chouzier, Afanasiev, Vrinat, Cseri, & Roy-Auberger, 2006; Chouzier, Vrinat, Cseri, Roy-Auberger, & Afanasiev, 2011), and oxide nanoparticles (Yufanyi, Tendo, Ondoh, & Mbadcam, 2014).

2. Method

2.1 Materials

$Co(NO_3)_2.6H_2O$, $Zn(NO_3)_2.6H_2O$, hexamethylenetetramine and ethanol were obtained from Sigma Aldrich. All the chemicals were of analytical grade and were used as obtained without further purification.

2.2 Synthesis of Metal(II) - HMTA Complex

The precursors were synthesized according to a procedure previously reported for a polymeric $Co(HMTA)_2(NO_3)_2(H_2O)_2$ complex, with slight modifications (Ndifon et al., 2009).

HMTA (4 mmol; 0.5608 g) was dissolved in 20 mL of ethanol/water mixture (6:1 v/v) by sonicating for 20 minutes, at room temperature. The solution was magnetically stirred while stoichiometric amounts of the metal nitrate (2 mmol) in 10 mL of ethanol was added drop wise to the HMTA solution and the mixture was stirred for two hours. The pink precipitate (Co-HMTA) and the white precipitate (Zn-HMTA) that were obtained were filtered, washed several times with 99% ethanol and dried in a desiccator over silica gel. Pink crystals (Co-HMTA) and colourless crystals (Zn-HMTA) suitable for single crystal XRD were obtained from the filtrates within two weeks.

2.3 Synthesis of Cobalt and Zinc Oxide Nanoparticles

The dry M-HMTA complex (0.5 g) was ground and placed in a ceramic crucible that had previously been washed, dried and weighed. The crucible was placed into a furnace and heated at a ramp rate of 5˚C per minute until the desired temperature was reached (500°C) and calcined in the presence of air for two hours. The sample was allowed to cool slowly to room temperature. The obtained black powder (case of cobalt) and the white product (case of zinc) were weighed and could easily be re-dispersed in water and ethanol. The samples are referred to as Co_3O_4-500 and ZnO-500.

2.4 Characterisation

Elemental analysis (C, H, N) of the precursor was carried out on a Flash 2000 Thermo Scientific analyser while the FT-IR spectra were recorded from 4000 to 400 cm^{-1} on a PerkinElmer Spectrum Two universal attenuated total reflectance Fourier transform infrared (UATR-FT-IR) spectrometer.

Single crystal X-ray data were collected using a graphite monochromatic Mo-Kα radiation (λ=1.54178 Å) from a Bruker APEX diffractometer. The structures were solved by direct methods and refined by full-matrix least squares on F^2 (Sheldrick, 1997a, 1997b). The non-hydrogen atoms were refined anisotropically. H atoms were included in calculated positions with C-H lengths of 0.95(CH), assigned isotropic thermal parameters and allowed to ride on their parent carbon atoms. All calculations were carried out using the SHELXTL package (Bruker, 2001).

Thermogravimetric measurements were obtained using a Pyris 6 PerkinElmer TGA 4000 thermal analyser. The TGA analyses were conducted between 30 and 900°C under nitrogen atmosphere at a flow rate of 20 mL/min and a temperature ramp of 10°C/min. The XRD diffractogram were recorded on a Bruker D8 Advance X-ray diffractometer using a Cu Kα radiation source (λ = 0.15406 nm, 40 kV and 40 mA). Scans were taken over the 2θ range from 10º to 100º in steps of 0.01º at room temperature in open quartz sample holders. The phases were identified with the help of the Bruker DIFFRACplus evaluation software in combination with the ICDD powder diffraction data base (International Centre for Diffraction Data). FESEM images and energy dispersive X-ray (EDX) spectra were obtained on a JEOL JSM-7600F field-emission scanning electron microscope (FESEM), with a lens diameter of 800 mm^2 (Oxford Instruments Ltd, UK) coupled to a silicon drift energy-dispersive X-ray detector. Transmission electron microscopy (TEM) was performed on a JEOL JEM-2100F microscope using a maximum acceleration voltage of 200 kV from the field emission gun. The particle size distributions were determined from the TEM images using the ImageJ software. N_2-physisorption experiments for the determination of the total surface area and the average pore diameter were conducted on a Micromeritics ASAP 2020 instrument. Prior to the measurement, the samples were degassed at 200˚C for 6 h.

3. Results and Discussion

By careful choice of the precursor, coupled with a rational control of temperature and other conditions, nano-sized cobalt and zinc oxides were obtained by thermal decomposition of their corresponding hexamethylenetetramine (HMTA) complexes. These complexes were prepared in a single step, in high yield at room temperature.

The elemental analytical data of the precursors (Table 1) correspond closely to the empirical formulae $CoC_{12}H_{28}N_{10}O_8$ and $ZnC_{12}H_{44}N_{10}O_{16}$ which matches the structural formulae $[Co(HMTA)_2(H_2O)_2(NO_3)_2]$ and $[Zn(H_2O)_6](HMTA)_2(NO_3)_2·4H_2O$, respectively, for cobalt and zinc.

Table 1. Elemental analytical data of the complexes

Complex	Yield (%)	Colour	Elemental Analysis: % Found (% Calc.)		
			% C	% H	% N
$[Co(HMTA)_2(H_2O)_2(NO_3)_2]$	85	Pink crystals	28.73 (28.86)	5.82 (5.65)	27.56 (28.05)
$[Zn(H_2O)_6](HMTA)_2(NO_3)_2 \cdot 4H_2O$	78	Colourless crystals	22.21 (22.18)	6.74 (6.82)	21.23 (21.55)

3.1 X-ray Crystal Structure

The crystal structures of the precursors Co-HMTA and Zn-HMTA were found to be the same as those of the complexes $[Co(HMTA)_2(H_2O)_2(NO_3)_2]$ (Ndifon et al., 2009) and $[Zn(H_2O)_6](HMTA)_2(NO_3)_2 \cdot 4H_2O$ (Singh et al., 2008) respectively, found in literature.

3.2 FTIR Analyses of the Precursor Complexes

The relevant infrared bands of HMTA and the precursor complexes are listed in Table 2, while the FTIR spectra of the precursor complexes and the corresponding oxides are shown in Figure 1. The broad bands at 3400 - 3501 cm^{-1} in the spectra of M-HMTA are attributed to $\nu(OH)$ of coordinated water , while that at 3383 cm^{-1} is assigned to $\nu(OH)$ of lattice water (Hee Ng, Guan Teoh, Moris, & Yang Yap, 2004). The band at 1235 cm^{-1}, assigned to the $\nu(CH_2)$ rocking vibration of the free HMTA ligand is observed at 1238 cm^{-1} in the Zn-HMTA complex, while it is split into 1240 and 1227 cm^{-1} in the Co-HMTA precursor suggesting that HMTA is coordinated to the cobalt ion (Ndifon et al., 2009). Strong prominent peaks at 812 and 1000 cm^{-1} due to the C-N stretching vibration of HMTA are shifted to 818-819 cm^{-1} and 1002 cm^{-1}, respectively in the Co-HMTA and Zn-HMTA precursor complexes (Jensen, 2002). The weak band observed at 1780 cm^{-1} shows the coordination of a monodentate nitrate ion, Co-NO$_3$ (Ndifon et al., 2009). The coordination of water molecules is also indicated by the IR bands in the region 400–600 cm^{-1}, assigned to M-H$_2$O (Ndifon et al., 2009).

Table 2. Relevant FTIR bands of HMTA and the M-HMTA precursor complexes

HMTA	$[Co(HMTA)_2(NO_3)_2(H_2O)_2]$	$[Zn(H_2O)_6](HMTA)_2(NO_3)_2 \cdot 4H_2O$	Band Assignments
-	3501	3480	$\nu(OH)$ (coordinated water)
-	-	3383	$\nu(OH)$ (lattice water)
2955	-	2970	$\nu(CH_2)$
-	1780	-	Co-NO$_3$
-	1675	1674	HOH bend (lattice water)
1457	1475	1463	$\nu(CH_2)$ scissor (HMTA)
1370	1349	1343	$\nu(CH_2)$ wag (HMTA)
1236	1240	1238	$\nu(CH_2)$ rock (HMTA)
	1227		
1000	1002	1002	$\nu(CN)$ stretch (HMTA)
811	819	818	$\nu(CN)$ stretch (HMTA)
670	682	687	N-C-N bend (HMTA)
-	504	505	M-O stretch

3.3 Thermogravimetric Analysis

The TG curves of the precursor complexes are presented in Figure 2 and summarised in Table 3. The curves indicate that both complexes decompose in more than one step to give the metal oxides. The thermal decomposition of these precursors is accompanied by the evolution of a mixture of gases.
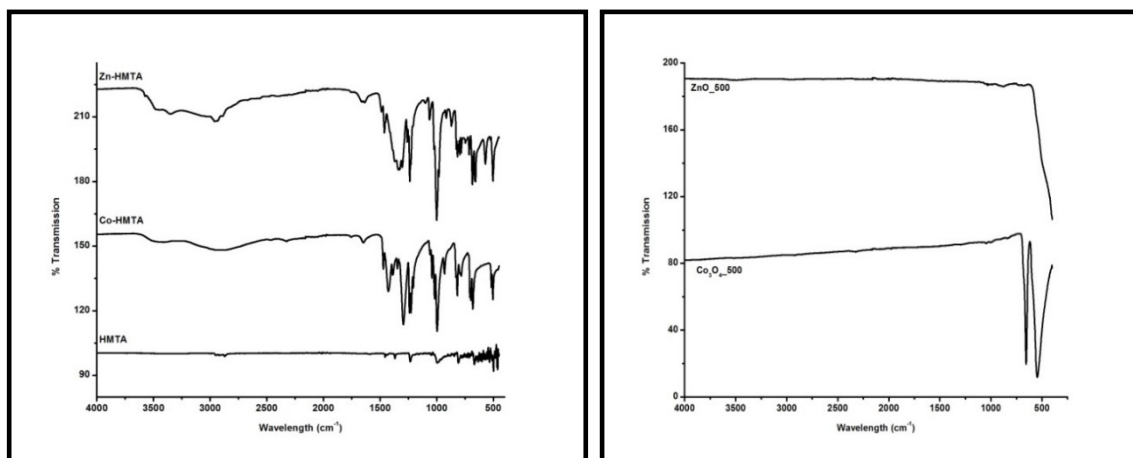
Figure 1. FTIR spectra of HMTA, the precursor complexes and the oxide nanoparticles

Table 3. Thermal decomposition data for the precursor complexes

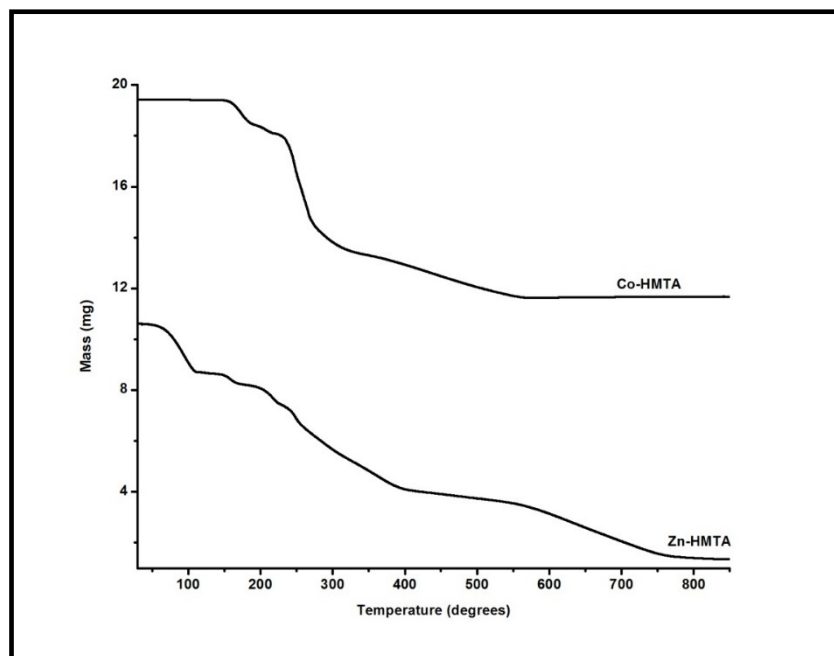| Complex	Step	Temperature range (ºC)	% Mass Loss	
			Obs.	Calc.
[Co(HMTA)$_2$(NO$_3$)$_2$(H$_2$O)$_2$]	I	135 - 198	8.5	10.02
	II	200 - 315	53.6	56
	III	320 - 540	13.6	12.4
[Zn(H$_2$O)$_6$](HMTA)$_2$(NO$_3$)$_2$·4H$_2$O	I	40 - 100	14.8	13.8
	II	105 - 153	4.71	5.5
	III	160 – 420	42.4	43.1
	IV	420 - 740	23.4	27.4

Figure 2. TG curves of the precursor complexes

For the Co-HMTA, the mass loss of 8.5% in the temperature region from 135 - 198ºC is most probably due to the loss of two coordinated water molecules (10.02 %). The major mass loss of 53.6% takes place in the range 200 - 315ºC, and is attributed to the complete decomposition of HMTA (56%) in the form of various gases (Afanasiev et al., 2008). In the range 320 – 540ºC we have another distinctive decomposition step with a mass loss of 13.6% which can be assigned to the decomposition of the nitrate. A stable mass is reached at 540ºC. The calcination temperature was chosen as 500°C from the derivative TG plot.

Considering the decomposition of the Zn-HMTA complex, the mass loss of 14.8% in the temperature region from 50 – 102ºC is attributed to the loss of five water molecules (13.8%). The next decomposition step in the range 105 – 155ºC with mass loss of 4.71% is probably due to the loss of two coordinated water molecules (5.5%). In the temperature range 155 – 380ºC which, from the derivative TG plots, consists of several overlapping decomposition steps, there is a major mass loss of 42.4% which can be assigned to the decomposition of two HMTA molecules (43.1%) (Afanasiev et al., 2008; Hee Ng et al., 2004). The decomposition step in the range 400 – 740ºC involves a mass loss of 23.4% which can be assigned to the decomposition of the two nitrates and two water molecules (calc. 27.4%). A residual mass of 14.6% is observed at 740ºC which is probably due to zinc metal (10.1%).

The last decomposition step for Zn-HMTA is probably accompanied by the reduction of ZnO to zinc by carbon from 570˚C. From the Ellingham diagram, carbon will reduce zinc oxide above 950˚C for CO/CO$_2$ ratio of 1. In an oxygen deficient atmosphere, the ratio will probably decrease pushing the reduction temperature to the observed lower value.

The calcination temperature was chosen as 500ºC from the derivative TG plot which indicates that 600°C is the optimum temperature. The decomposition pattern of the Zn-HMTA complex is slightly different from that reported in the literature, where the complex decomposes in two major steps in the temperature ranges 65 – 100ºC and 600 – 645ºC (Singh et al., 2008).

3.4 Structural Characterisation of the Oxide Nanoparticles

The FTIR spectra of the oxides are shown in Figure 1. The spectra show bands in the 500 - 650 cm^{-1} region which are attributed to the stretching vibration of the M-O bond. The bands at 547 and 645 cm^{-1} for cobalt oxide, suggest the formation of spinel Co_3O_4 that is $(Co^{2+})(Co^{3+})_2(O^{2-})_4$ (Makhlouf, Abu-Zied, & Mansoure, 2013; Nguimezong et al., 2014). These bands have been attributed to the (Co^{2+})-O-(Co^{3+}) and to (Co^{3+})-O-(Co^{3+}) vibrations, respectively (Makhlouf et al., 2013; Nguimezong et al., 2014).

The cobalt oxide and zinc oxide nanoparticles were obtained by thermal decomposition of their respective M-HMTA precursors at 500 ºC. The XRD patterns of Co_3O_4 and ZnO (Figure 3) indicate that pure and crystalline metal oxide phases are formed in both cases. The samples have well defined diffraction patterns. The peaks for Co_3O_4 correspond to the (111), (220), (311), (222), (400), (511) and (440) crystals planes and match the spinel structure of cubic Co_3O_4 JCPDS card no 43-1003 (space group: Fd3m) (Lester et al., 2012). The peaks for ZnO correspond to the (100), (002), (101), (102), (110), (103), (200), (112), and (201) crystal planes and match the wurtzite structure of hexagonal ZnO JCPDS card no. 36-1451 (Zhang, Ram, Stefanakos, & Goswami, 2012). The average crystallite sizes determined by the Debye-Scherrer equation (Klug & (Eds.), 1974) from the peak-width at half-height of the (311) peak for Co_3O_4 and the (101) peaks for ZnO, were found to be 23 and 32.5 nm for Co_3O_4-500 and ZnO-500, respectively.

The morphologies and other structural features of the precursor complexes, Co_3O_4-500 and ZnO-500 samples were determined by FESEM, TEM and SAED. The FESEM images (Figure 4) show that the precursor complexes Co-HMTA (Figure 4a) and Zn-HMTA (Figure 4b) have spike-like and bar-like morphologies, respectively, while Co_3O_4-500 (Figure 4c) is highly porous and foam-like. The ZnO-500 particles (Figure 4d) exhibit a rod-like shape. The formation of highly porous foam can be attributed to the large amounts of gases evolved when HMTA and nitrates decompose (Afanasiev et al., 2008).

The corresponding TEM images (Figure 5) confirm cube-like (Co_3O_4) and hexagonal-prism like (ZnO) morphologies, with average particle sizes of 19.6 and 64.5 nm, respectively. The average particle diameter was determined after a log normal fitting of the data obtained from the TEM images. The SAED images (Figure 5) show patterns corresponding to the polycrystalline nature of the Co_3O_4 and ZnO formed.
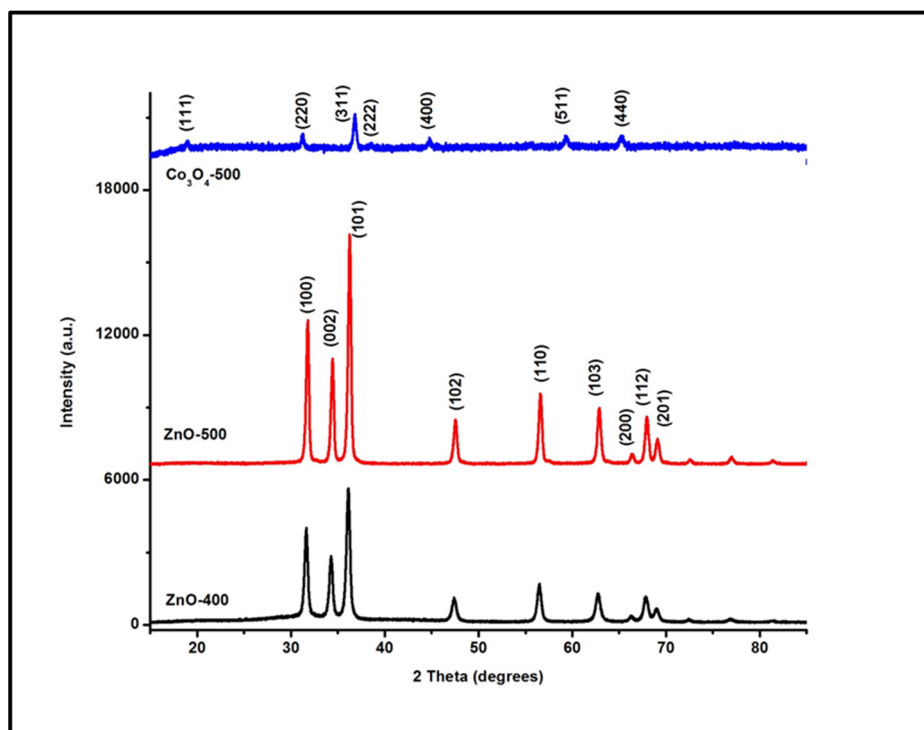
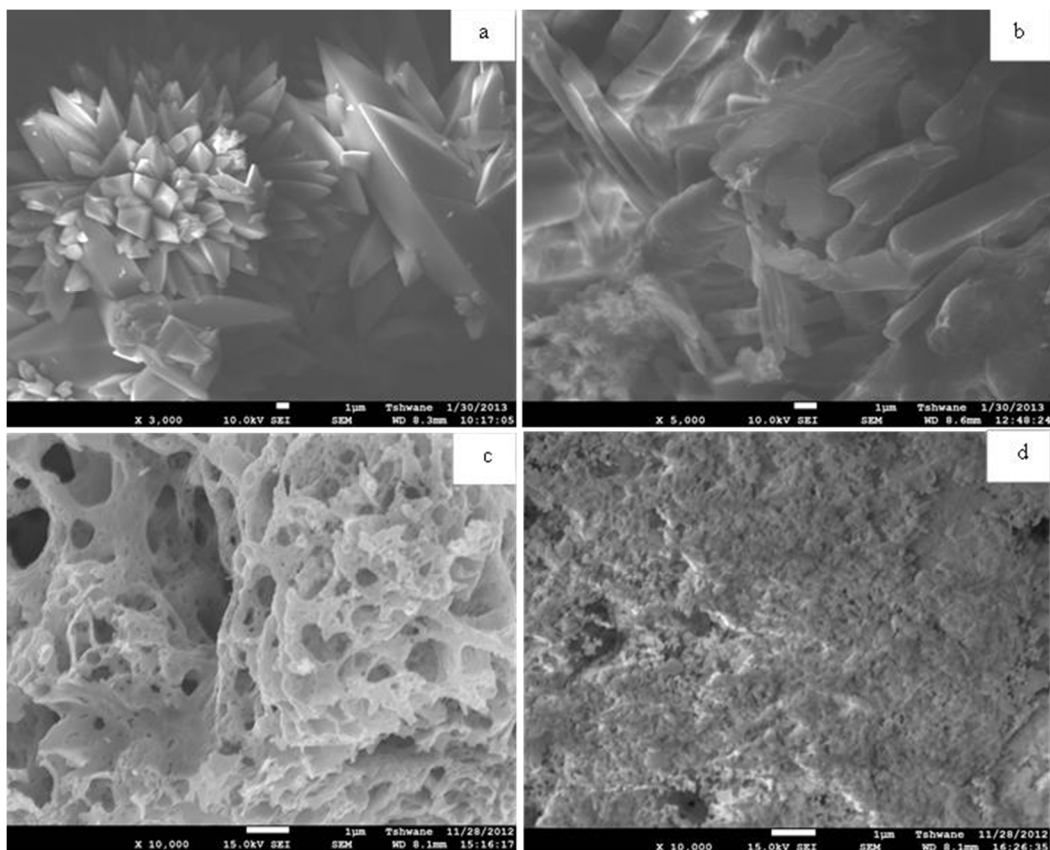Figure 3. XRD patterns of Co₃O₄-500, ZnO-400 and ZnO-500 obtained by thermal decomposition

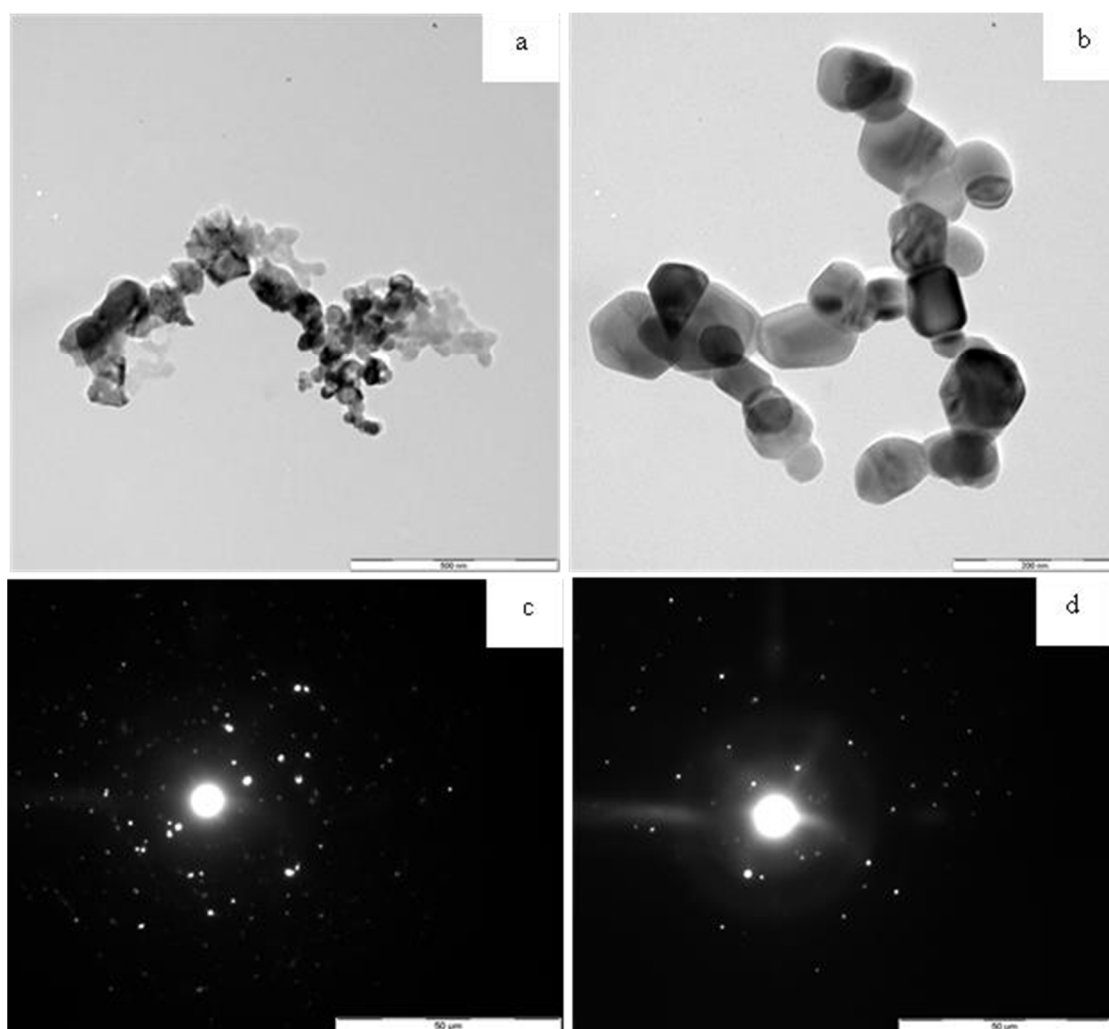Figure 4. FESEM images of (a) Co-HMTA precursor; (b) Zn-HMTA precursor; (c) Co3O4-500 and (d) ZnO-500

Figure 5. HRTEM images of (a) Co3O4 and (b) ZnO; SAED images of (c) Co3O4 and (d) ZnO

The particle size distributions and average particle sizes for Co_3O_4-500 and ZnO-500 nanoparticles are shown in Figure 6. From this histogram it is observed that the particle sizes for Co_3O_4-500 and ZnO-500 vary from 15 – 25 nm and 45 – 85 nm, respectively. The average particle sizes from TEM are consistent with values obtained by XRD.
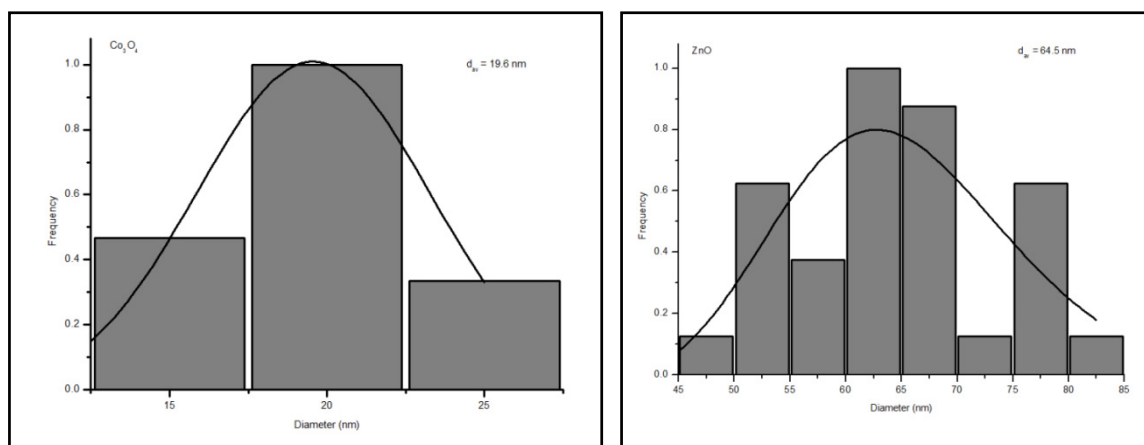

Figure 6. Particle size distribution for Co_3O_4-500 and ZnO-500 nanoparticles

For comparison, the precursors, decomposition time and temperatures used to obtain Co_3O_4-500 and ZnO-500 nanoparticles by thermal decomposition, with various morphologies and sizes, found in the literature are listed in Table 4. The results show that cube-like (Co_3O_4-500) and hexagonal-like (ZnO-500) nanoparticles with average particle sizes of 19.6 and 64.5 nm, respectively obtained from the M-HMTA precursors of this study compares favorably with those obtained from other starting materials. It can also be observed from Table 4 that our starting materials are the simplest, most readily available, and very cost-effective.

Table 4. Particle sizes (TEM) and morphologies of Co_3O_4-500 and ZnO-500 nanoparticles prepared by the thermal decomposition of various precursors at different calcination temperatures

Precursor	Calcination		Particle Size (TEM) (nm)	Morphology	Ref.
	Time (h)	Temp. (°C)			
$Co(NO_3)_2 \cdot 6H_2O + (NH_4)_2CO_3$	2 - 3	300 -500	12 - 14	Pseudo-hexagonal	(de Rivas et al., 2012)
$Co(acetate)_2$ + oxalic acid	2 -3	500	12 - 14	Pseudo-hexagonal	(de Rivas et al., 2012)
$CoCl_2$ or $Co(NO_3)_2$ or $Co(acetate)_2$ +urea + CTAB	6	400 - 500	30 -39	Rounded and squared	(Nassar & Ahmed, 2011)
$Co(NO_3)_2 + (NH_4)_2OX$	6	400	25	microdiscs	(Che et al., 2013)
$[Co(NH_3)CO_3]NO_3 \cdot 0.5H_2O$	1	175 - 300	10	Quasi-spherical	(Farhadi & Safabakhsh, 2012)
$Zn_4(SO_4)(OH)_6 \cdot 0.5 \ H_2O$	1	825	92	Spherical	(Darezereshki et al., 2011)
$[Zn(H_2O)_6](HMTA)_2(NO_3)_2 \cdot 4H_2O$	2	500	64.5	Hexagonal-like	This work

3.5 Surface Area and Pore Size Analyses

The surface areas of Co_3O_4-500 and ZnO-500 were determined by N_2 physisorption. All isotherms (Figure 7) were typical of mesoporous solids (type IV), for which both the surface area and the pore size distribution can be determined (Greg & Sing, 1982). The hysteresis loops (according to the IUPAC classification) were of type H1, which are often obtained for agglomerates or compacts of spheroidal particles of fairly uniform size and array (Greg & Sing, 1982). The BET surface areas of the samples (according to Brunauer, Emmett and Teller) are 5.1 and 10.4 m^2/g, respectively. The corresponding Barrett-Joyner-Halenda (BJH) desorption pore sizes are 25 and 12 nm. Table 5 summarizes the results.
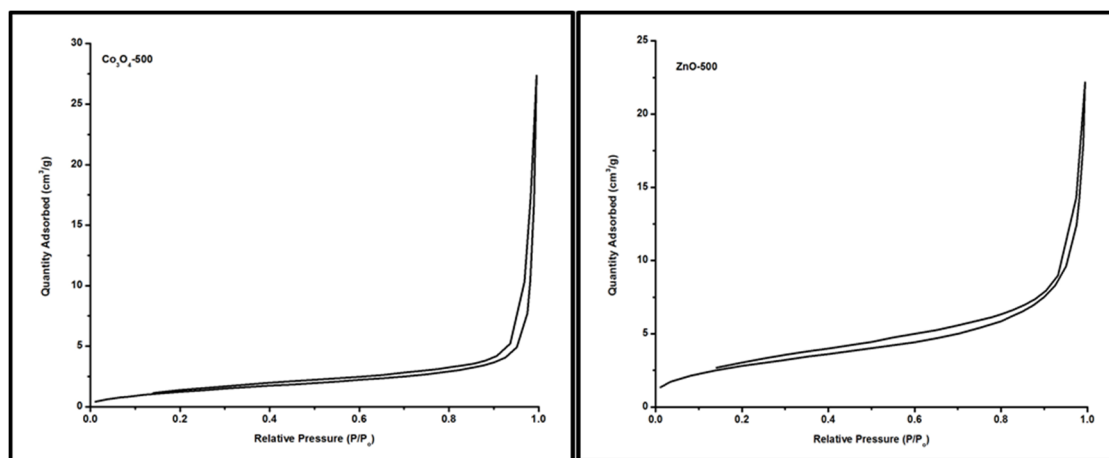

Figure 7. N_2 adsorption/desorption isotherms for the Co_3O_4-500 and ZnO-500 samples

Table 5. Surface area, average pore diameter (APD) and pore volume of the samples

Sample	BET Surface Area (m^2/g)	BJH Desorption APD (nm)	Pore Volume (cm^3/g)
Co_3O_4-500	5.1	25	0.043
ZnO-500	10.4	12	0.035

4. Conclusion

Pure and crystalline Co_3O_4 and ZnO nanoparticles, with defined morphologies, have been obtained from their corresponding metal-HMTA complexes by thermal decomposition. While Co_3O_4 is foam-like, ZnO nanoparticles have a rod-like shape according to FESEM. The corresponding TEM images confirm cube-like (Co_3O_4) and hexagonal-prism like (ZnO) morphologies, with average particle sizes of 19.6 and 64.5 nm, respectively. All oxide particles were mesoporous with BET surface areas of 5.1 m^2/g (Co_3O_4) and 10.4 m^2/g (ZnO). This technique that makes use of simple and readily available precursors for metal oxide nanoparticle synthesis could be extended to the synthesis of other metal oxide nanoparticles.

Acknowledgements

References

Afanasiev, P., Chouzier, S., Czeri, T., Pilet, G., Pichon, C., Roy, M., & Vrinat, M. (2008). Nickel and Cobalt Hexamethylentetramine Complexes $(NO_3)_2Me(H_2O)_6(HMTA)_2 \cdot 4H_2O$ (Me = Co^{2+}, Ni^{2+}): New Molecular Precursors for the Preparation of Metal Dispersions. *Inorganic Chemistry, 47*(7), 2303-2311. http://dx.doi.org/10.1021/ic7013013

Aghababazadeh, R., Mazinani, B., Mirhabibi, A., & Tamizifar, M. (2006). ZnO Nanoparticles Synthesised by mechanochemical processing. *Journal of Physics: Conference Series, 26*(1), 312.

Ahmad, T., Ganguly, A., Ahmed, J., Ganguli, A. K., & Alhartomy, O. A. A. (2011). Nanorods of transition metal oxalates: A versatile route to the oxide nanoparticles. *Arabian Journal of Chemistry, 4*(2), 125-134. http://dx.doi.org/10.1016/j.arabjc.2010.06.041

Banerjee, P., Chakrabarti, S., Maitra, S., & Dutta, B. K. (2012). Zinc oxide nano-particles: Sonochemical synthesis, characterization and application for photo-remediation of heavy metal. *Ultrasonics Sonochemistry, 19*(1), 85-93. http://dx.doi.org/10.1016/j.ultsonch.2011.05.007

Bruker. (2001). SMART (Version 5.625), SADABS (Version 2.03a) and SHELXTL (Version 6.12). Madison, Wisconsin, USA: Bruker AXS Inc.

Che, H., Liu, A., Fu, Q., & Jiang, R. (2013). Facile synthesis of porous cobalt oxide microdiscs and their catalytic property in CO oxidation. *Materials Letters, 93*(0), 240-242. http://dx.doi.org/10.1016/j.matlet.2012.11.108

Chouzier, S., Afanasiev, P., Vrinat, M., Cseri, T., & Roy-Auberger, M. (2006). One-step synthesis of dispersed bimetallic carbides and nitrides from transition metals hexamethylenetetramine complexes. *Journal of Solid State Chemistry, 179*(11), 3314-3323. http://dx.doi.org/10.1016/j.jssc.2006.06.026

Chouzier, S., Vrinat, M., Cseri, T., Roy-Auberger, M., & Afanasiev, P. (2011). HDS and HDN activity of (Ni,Co)Mo binary and ternary nitrides prepared by decomposition of hexamethylenetetramine complexes. *Applied Catalysis A: General, 400*(1–2), 82-90. http://dx.doi.org/10.1016/j.apcata.2011.04.023

Dakhlaoui, A., Jendoubi, M., Smiri, L. S., Kanaev, A., & Jouini, N. (2009). Synthesis, characterization and optical properties of ZnO nanoparticles with controlled size and morphology. *Journal of Crystal Growth, 311*(16), 3989-3996. http://dx.doi.org/10.1016/j.jcrysgro.2009.06.028

Darezereshki, E., Alizadeh, M., Bakhtiari, F., Schaffie, M., & Ranjbar, M. (2011). A novel thermal decomposition method for the synthesis of ZnO nanoparticles from low concentration $ZnSO_4$ solutions. *Applied Clay Science, 54*(1), 107-111. http://dx.doi.org/10.1016/j.clay.2011.07.023

de Rivas, B., López-Fonseca, R., Jiménez-González, C., & Gutiérrez-Ortiz, J. I. (2012). Highly active behaviour of nanocrystalline Co_3O_4 from oxalate nanorods in the oxidation of chlorinated short chain alkanes. *Chemical Engineering Journal, 184*(0), 184-192. http://dx.doi.org/10.1016/j.cej.2012.01.027

Devan, R. S., Patil, R. A., Lin, J.-H., & Ma, Y.-R. (2012). One-Dimensional Metal-Oxide Nanostructures: Recent Developments in Synthesis, Characterization, and Applications. *Advanced Functional Materials, 22*(16), 3326-3370. http://dx.doi.org/10.1002/adfm.201201008

Faisal, M., Khan, S. B., Rahman, M. M., Jamal, A., & Abdullah, M. M. (2012). Fabrication of ZnO nanoparticles based sensitive methanol sensor and efficient photocatalyst. *Applied Surface Science, 258*(19), 7515-7522. http://dx.doi.org/10.1016/j.apsusc.2012.04.075

Farhadi, S., & Safabakhsh, J. (2012). Solid-state thermal decomposition of the $[Co(NH_3)_5CO_3]NO_3 \cdot 0.5H_2O$ complex: A simple, rapid and low-temperature synthetic route to Co_3O_4 nanoparticles. *Journal of Alloys and Compounds, 515*(0), 180-185. http://dx.doi.org/10.1016/j.jallcom.2011.11.135

Fu, L., & Fu, Z. (2015). *Plectranthus amboinicus* leaf extract-assisted biosynthesis of ZnO nanoparticles and their photocatalytic activity. *Ceramics International, 41*(2, Part A), 2492-2496. http://dx.doi.org/10.1016/j.ceramint.2014.10.069

Gomez, J. L., & Tigli, O. (2013). Zinc oxide nanostructures: from growth to application. *Journal of Materials Science, 48*(2), 612-624. http://dx.doi.org/10.1007/s10853-012-6938-5

Greene, L. E., Yuhas, B. D., Law, M., Zitoun, D., & Yang, P. (2006). Solution-Grown Zinc Oxide Nanowires. *Inorganic Chemistry, 45*(19), 7535-7543. http://dx.doi.org/10.1021/ic0601900

Greg, S. J., & Sing, K. S. W. (1982). *Adsorption, Surface Area and Porosity* (2nd ed.): Academic Press.

Guo, J., & Peng, C. (2015). Synthesis of ZnO nanoparticles with a novel combustion method and their C_2H_5OH gas sensing properties. *Ceramics International, 41*(2, Part A), 2180-2186. http://dx.doi.org/10.1016/j.ceramint.2014.10.017

Hee Ng, C., Guan Teoh, S., Moris, N., & Yang Yap, S. (2004). Structural, infrared spectral and thermogravimetric analysis of a hydrogen-bonded assembly of cobalt(II) and nickel(II) mixed complex cations with hexamethylenetetraamine and aqua ligands: $\{[M(hmt)_2(H_2O)_4][M(H_2O)_6]\}(SO_4)_2 \cdot 6H_2O$. *Journal of Coordination Chemistry, 57*(12), 1037-1046. http://dx.doi.org/10.1080/00958970412331281791

Hirai, T., & Asada, Y. (2005). Preparation of ZnO nanoparticles in a reverse micellar system and their photoluminescence properties. *Journal of Colloid and Interface Science, 284*(1), 184-189. http://dx.doi.org/10.1016/j.jcis.2004.09.069

Huang, Y., Chen, C., An, C., Xu, C., Xu, Y., Wang, Y., . . . Yuan, H. (2014). Synthesis of Cobalt based Complexes and conversion to Co_3O_4 nanoparticles as a high performance anode for lithium ion battery. *Electrochimica Acta, 145*(0), 34-39. http://dx.doi.org/10.1016/j.electacta.2014.08.085

Jensen, J. O. (2002). Vibrational frequencies and structural determinations of hexamethylenetetraamine. *Spectrochimica Acta Part A: Molecular and Biomolecular Spectroscopy, 58*(7), 1347-1364. http://dx.doi.org/10.1016/S1386-1425(01)00585-6

Kahn, M. L., Glaria, A., Pages, C., Monge, M., Saint Macary, L., Maisonnat, A., & Chaudret, B. (2009). Organometallic chemistry: an alternative approach towards metal oxide nanoparticles. *Journal of Materials Chemistry, 19*(24), 4044-4060. http://dx.doi.org/10.1039/b818935h

Karami, B., Eskandari, K., Khodabakhshi, S., Hoseini, S. J., & Hashemian, F. (2013). Green synthesis of three substituted methane derivatives by employing ZnO nanoparticles as a powerful and recyclable catalyst. *RSC Advances, 3*(45), 23335-23342. http://dx.doi.org/10.1039/c3ra42993h

Khalaji, A. D., Nikookar, M., Fejfarova, K., & Dusek, M. (2014). Synthesis of new cobalt(III) Schiff base complex: A new precursor for preparation Co_3O_4 nanoparticles via solid-state thermal decomposition. *Journal of Molecular Structure, 1071*(0), 6-10. http://dx.doi.org/10.1016/j.molstruc.2014.04.043

Klug, H. P., & (Eds.), L. E. A. (1974). *X-ray Diffraction Procedures for Polycrystalline and Amorphous Materials*. New York: Wiley.

Lester, E., Aksomaityte, G., Li, J., Gomez, S., Gonzalez-Gonzalez, J., & Poliakoff, M. (2012). Controlled continuous hydrothermal synthesis of cobalt oxide (Co_3O_4) nanoparticles. *Progress in Crystal Growth and Characterization of Materials, 58*(1), 3-13. http://dx.doi.org/10.1016/j.pcrysgrow.2011.10.008

Li, X., Dou, W., & Bao, N. (2012). Hydrothermal synthesis of tubular ZnO materials. *Materials Letters, 68*(0), 140-142. http://dx.doi.org/10.1016/j.matlet.2011.10.036

Makhlouf, M. T., Abu-Zied, B. M., & Mansoure, T. H. (2013). Direct Fabrication of Cobalt Oxide Nanoparticles Employing Sucrose as a Combustion Fuel. *Journal of Nanoparticles, 2013, Article ID 384350*, 7 pages. http://dx.doi.org/10.1155/2013/384350

Moro, F., Yu Tang, S. V., Tuna, F., & Lester, E. (2013). Magnetic properties of cobalt oxide nanoparticles synthesised by a continuous hydrothermal method. *Journal of Magnetism and Magnetic Materials, 348*, 1-7. http://dx.doi.org/10.1016/j.jmmm.2013.07.064

Nassar, M. Y., & Ahmed, I. S. (2011). Hydrothermal synthesis of cobalt carbonates using different counter ions: An efficient precursor to nano-sized cobalt oxide (Co_3O_4). *Polyhedron, 30*(15), 2431-2437. http://dx.doi.org/10.1016/j.poly.2011.05.039

Ndifon, P. T., Agwara, M. O., Paboudam, A. G., Yufanyi, D. M., Ngoune, J., Galindo, A., Alvarez, E., Mohamadou, A. (2009). Synthesis, characterisation and crystal structure of a cobalt(II)-hexamethylenetetramine coordination polymer. *Transition Metal Chemistry, 34*(7), 745-750. http://dx.doi.org/10.1007/s11243-009-9257-1

Nguimezong, M. B. N., Foba-Tendo, J., Yufanyi, D. M., Etape, E. P., Eko, J. N., & Ngolui, L. J. (2014). Averrhoa carambola: A Renewable Source of Oxalic Acid for the Facile and Green Synthesis of Divalent Metal (Fe,

Co, Ni, Zn, and Cu) Oxalates and Oxide Nanoparticles. *Journal of Applied Chemistry, 2014, Article ID 767695*, 9 pages. http://dx.doi.org/10.1155/2014/767695

Niederberger, M. (2007). Nonaqueous Sol–Gel Routes to Metal Oxide Nanoparticles. *Accounts of Chemical Research, 40*(9), 793-800. http://dx.doi.org/10.1021/ar600035e

Pál, E., Hornok, V., Kun, R., Chernyshev, V., Seemann, T., Dékány, I., & Busse, M. (2012). Growth of raspberry-, prism- and flower-like ZnO particles using template-free low-temperature hydrothermal method and their application as humidity sensors. *Journal of Nanoparticle Research C7 - 1002, 14*(8), 1-14. http://dx.doi.org/10.1007/s11051-012-1002-6

Palacios-Hernández, T., Hirata-Flores, G. A., Contreras-López, O. E., Mendoza-Sánchez, M. E., Valeriano-Arreola, I., González-Vergara, E., & Méndez-Rojas, M. A. (2012). Synthesis of Cu and Co metal oxide nanoparticles from thermal decomposition of tartrate complexes. *Inorganica Chimica Acta, 392*(0), 277-282. http://dx.doi.org/10.1016/j.ica.2012.03.039

Rajesh, D., Vara Lakshmi, B., & Sunandana, C. S. (2012). Two-step synthesis and characterization of ZnO nanoparticles. *Physica B: Condensed Matter, 407*(23), 4537-4539. http://dx.doi.org/10.1016/j.physb.2012.07.050

Romo, L. E., Saade, H., Puente, B., Lopez, M. L., Betancourt, R., & Lopez, R. G. (2011). Precipitation of Zinc Oxide Nanoparticles in Bicontinuous Microemulsions. *Journal of Nanomaterials, 2011, Article ID 145963*, 9 pages. http://dx.doi.org/10.1155/2011/145963

Rui, X., Tan, H., Sim, D., Liu, W., Xu, C., Hng, H. H., ... Yan, Q. (2013). Template-free synthesis of urchin-like Co_3O_4 hollow spheres with good lithium storage properties. *Journal of Power Sources, 222*(0), 97-102. http://dx.doi.org/10.1016/j.jpowsour.2012.08.094

Sharma, G., & Jeevanandam, P. (2013). Synthesis of MgO supported Co_3O_4 nanoparticles by a novel thermal decomposition approach and studies on their magnetic properties. *Microporous and Mesoporous Materials, 165*(0), 55-62. http://dx.doi.org/10.1016/j.micromeso.2012.07.034

Sheldrick, G. M. (1997a). SHELXL97, Program for crystal structure refinement. University of Göttingen, Germany.

Sheldrick, G. M. (1997b). SHELXS97, Program for Crystal Structure solution. University of Göttingen, Germany.

Singh, G., Baranwal, B. P., Kapoor, I. P. S., Kumar, D., Singh, C. P., & Fröhlich, R. (2008). Some transition metal nitrate complexes with hexamethylenetetramine: Part LV. Preparation, X-ray crystallography and thermal decomposition. *Journal of Thermal Analysis and Calorimetry, 91*(3), 971-977. http://dx.doi.org/10.1007/s10973-007-8615-5

Vijayakumar, S., Ponnalagi, A. K., Nagamuthu, S., & Muralidharan, G. (2013). Microwave assisted synthesis of Co_3O_4 nanoparticles for high-performance supercapacitors. *Electrochimica Acta, 106*(0), 500-505. http://dx.doi.org/10.1016/j.electacta.2013.05.121

Warang, T., Patel, N., Santini, A., Bazzanella, N., Kale, A., & Miotello, A. (2012). Pulsed laser deposition of Co_3O_4 nanoparticles assembled coating: Role of substrate temperature to tailor disordered to crystalline phase and related photocatalytic activity in degradation of methylene blue. *Applied Catalysis A: General, 423–424*(0), 21-27. http://dx.doi.org/10.1016/j.apcata.2012.02.037

Xiong, H.-M., Ma, R.-Z., Wang, S.-F., & Xia, Y.-Y. (2011). Photoluminescent ZnO nanoparticles synthesized at the interface between air and triethylene glycol. *Journal of Materials Chemistry, 21*(9), 3178-3182. http://dx.doi.org/10.1039/c0jm02577a

Xu, H., Gao, L., Zhang, Q., Li, J., Diwu, J., Chou, X., ... Xue, C. (2014, Article ID 723057). Preparation Method of Co_3O_4 Nanoparticles Using Degreasing Cotton and Their Electrochemical Performances in Supercapacitors. *Journal of Nanomaterials, 2014*, 9 pages. http://dx.doi.org/10.1155/2014/723057

Xu, Y., Wang, C., Sun, Y., Zhang, G., & Gao, D. (2010). Fabrication and characterization of nearly monodisperse Co_3O_4 nanospheres. *Materials Letters, 64*(11), 1275-1278. http://dx.doi.org/10.1016/j.matlet.2010.03.007

Yufanyi, D. M., Tendo, J. F., Ondoh, A. M., & Mbadcam, J. K. (2014). CdO Nanoparticles by Thermal Decomposition of a Cadmium-Hexamethylenetetramine Complex. *Journal of Materials Science Research, 3*(3), 1-11. http://dx.doi.org/10.5539/jmsr.v3n3p1

Zhang, Y., Ram, M. K., Stefanakos, E. K., & Goswami, D. Y. (2012). Synthesis, Characterization, and Applications of ZnO Nanowires. *Journal of Nanomaterials, 2012, Article ID 624520*, 22 pages. http://dx.doi.org/10.1155/2012/624520

Copyrights